

PAPER

A Hybrid Technique for Thickness-Map Visualization of the Hip Cartilages in MRI

Mahdieh KHANMOHAMMADI[†], Reza AGHAIEZADEH ZOROOFI^{†*a)}, Takashi NISHII^{††}, Hisashi TANAKA^{†††}, *Nonmembers*, and Yoshinobu SATO^{†††}, *Member*

SUMMARY Quantification of the hip cartilages is clinically important. In this study, we propose an automatic technique for segmentation and visualization of the acetabular and femoral head cartilages based on clinically obtained multi-slice T1-weighted MR data and a hybrid approach. We follow a knowledge based approach by employing several features such as the anatomical shapes of the hip femoral and acetabular cartilages and corresponding image intensities. We estimate the center of the femoral head by a Hough transform and then automatically select the volume of interest. We then automatically segment the hip bones by a self-adaptive vector quantization technique. Next, we localize the articular central line by a modified canny edge detector based on the first and second derivative filters along the radial lines originated from the femoral head center and anatomical constraint. We then roughly segment the acetabular and femoral head cartilages using derivative images obtained in the previous step and a top-hat filter. Final masks of the acetabular and femoral head cartilages are automatically performed by employing the rough results, the estimated articular center line and the anatomical knowledge. Next, we generate a thickness map for each cartilage in the radial direction based on a Euclidian distance. Three dimensional pelvic bones, acetabular and femoral cartilages and corresponding thicknesses are overlaid and visualized. The techniques have been implemented in C++ and MATLAB environment. We have evaluated and clarified the usefulness of the proposed techniques in the presence of 40 clinical hips multi-slice MR images.

key words: *bone segmentation, singular value decomposition, Hough transform, directional derivative filters, cartilage segmentation, vector quantization, edge detection, thickness map visualization*

1. Introduction

Hip joint has a main role in human locomotion and bearing the body weight [1], [2]. The main functions of the hip joint articular cartilage include distribution of weight, frictionless motion and shock absorption. Consumption of drug and alcoholic liquor, senescence, inheritance and abnormal pressure results in deficiency of the normal functionality of the cartilage. The common causes of articular cartilage lesion are osteoarthritis and dysplasia. Late diagnosis of the osteoarthritis and dysplasia may result in limitation of the

joint function and painful stiffness [1]. Three dimensional visualization of the cartilage thickness is clinically useful for clinician and orthopedic surgeon to study the pathogenesis of joint dysfunction. This evaluation might be effective in diagnosis, treatment, planning and assessment of the orthopedic surgery [2], [3]. MR imaging is regarded as the clinical choice for cartilage imaging because of high contrast in soft tissue [4]. Cartilage imaging is often acquired by a fast suppressed T1-weighted 3D-gradient-echo sequence (SPGR). However, tissues with close gray level appear with different intensity in images obtained from MRI [5]–[12]. A normal hip joint is formed by the round ball-like upper end of the femur, the femoral head and a socket-like cavity, the acetabulum. The head of the femur is reinforced in its position by very powerful ligament [10]. The articular space between the femoral head and the acetabular cartilage is not explicitly distinguishable in normal joints. To allow clear separation of these cartilages on MR images, the original leg traction technique was used during MR imaging [12], [13]. Many research efforts have attempted to measure articular cartilage thickness using MRI data. However, most of them worked on knee joint and patellae and tibia cartilages [12]–[17]. In our previous attempts, we applied three dimensional directional derivative filters to enhance the cartilages boundaries [18]. We also developed an automatic technique for femoral head center estimation [10]. We segmented hip bony tissue based on Otsu's adaptive thresholding [19], and 3D morphological operations [20]. We classified the acetabular cartilage by a second order directional derivative and a B-Spline snake [20]. Based on the previous works, the purpose of this study is to develop techniques for thickness-map visualization of the acetabular and femoral head cartilages [9] below. In our approach, we first determine the central line of the articular space by exerting the canny edge detector operator on smoothed hip MR images in a slice by slice manner. We then segment the pelvic bones, i.e., the femoral head and acetabulum based on a vector quantization technique [21]–[27]. The articular cartilages are roughly segmented using a top-hat filter and Otsu's adaptive thresholding [28], [29]. We then employ the roughly segmented cartilages and articular central line to segment the hip cartilages from each other. Details of the proposed techniques are given in Sect. 2. In Sect. 3, we assess the techniques in the presence of the actual MR hip datasets. Discussions, concluding remarks and future directions are made in Sect. 4.

Manuscript received March 5, 2009.

[†]The authors are with Control and Intelligent Processing Center of Excellence, School of Electrical and Computer Engineering, College of Engineering, University of Tehran, North Kargar Ave., Tehran 14395–515, Iran.

^{††}The author is with the Department of Orthopedic Surgery, Osaka University, Graduate School of Medicine, Suita-shi, 565–0871 Japan.

^{†††}The authors are with the Department of Radiology, Osaka University, Graduate School of Medicine, Suita-shi, 565–0871 Japan.

*Corresponding author.

a) E-mail: zoroofi@ut.ac.ir

DOI: 10.1587/transinf.E92.D.2253

2. Proposed Techniques

In this section, we propose a hybrid multi-step technique for thickness-map visualization of the hip articular cartilage. In Sect. 2.1, based on our previous work [10], we introduce several preprocessing steps including dataset re-sampling and femoral head center estimation to obtain the hip volume of interest for further operations. A vector quantization approach for hip bones segmentation is proposed in Sect. 2.2. Details of the developed technique for articular-space central line estimation are explained in Sect. 2.3. In Sect. 2.4, based on the previous steps, we propose a method for femoral and acetabular cartilage segmentation. Cartilage thickness-map estimation and visualization are given in Sect. 2.5. Flow chart of the proposed techniques of this section is given in Fig. 1.

2.1 Preprocessing

In a typical MR data set of a hip joint, acetabular and

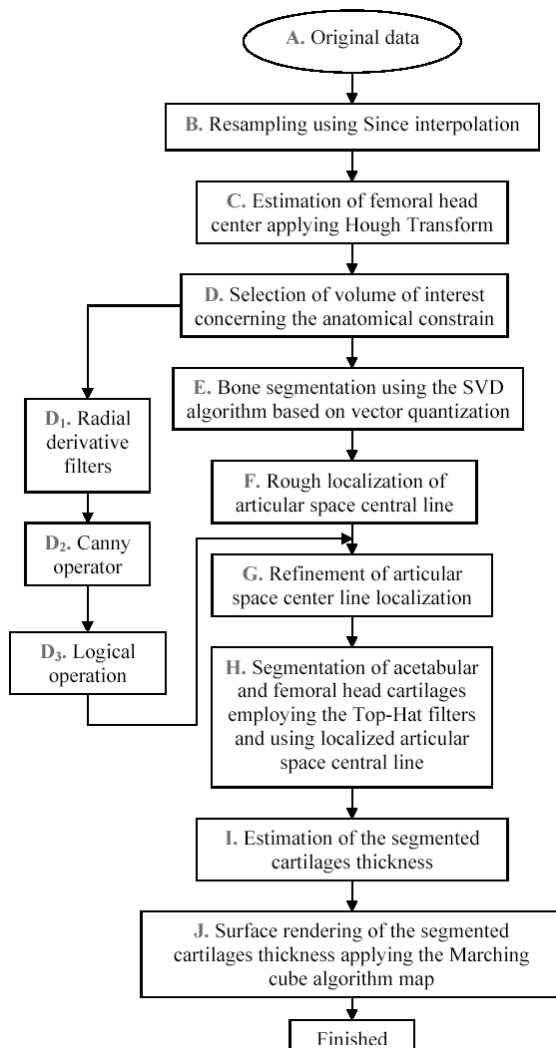


Fig. 1 Flowchart of the proposed techniques. See Sect. 2 for details.

femoral cartilages are attached to each other. To allow clear separation of acetabular and femoral cartilage on MR images, the original continuous leg traction technique was performed during MR imaging [9]. The voxel dimensions of the MR data in our study were non-cubic: $0.625 \times 0.625 \times 1.5 \text{ mm}^3$. We thus up-sampled the data in the sagittal direction by a Sinc interpolation, i.e., zero expansion (zero filling) in the frequency domain. The new voxel was a size of $0.625 \times 0.625 \times 0.625 \text{ mm}^3$. To provide sub-pixel accuracy for segmentation procedures, the obtained volume was up-sampled by a factor of two in all directions which resulted in new voxel size of $0.3125 \times 0.3125 \times 0.3125 \text{ mm}^3$ [20]. Figure 2 shows one slice of a typical data set after re-sampling.

The femoral head typically has a spherical shape with radius of around 20 to 25 mm. The center of the sphere approximated femoral head is found by utilizing this constraint in a Hough transform as follows

$$(X - X_0)^2 + (Y - Y_0)^2 + (Z - Z_0)^2 = a^2 \quad (1)$$

where (X_0, Y_0, Z_0) is the coordinate of femoral head center and a is the sphere radius.

In our method, the gradient vector and the restriction of the femoral head radius range are incorporated in the voting processes of the Hough transform. At each voxel position, when the gradient magnitude is large, the voting is performed to the candidate positions within distances between 20 and 30 mm toward the gradient vector direction. As shown in Fig. 2, in the acquired MR data, cartilage is of higher intensity than that of nearby bones. We calculate the first and second directional derivatives in the radial directions originating from the femoral head center [18] as follows.

$$\partial = f_x r_x + f_y r_y + f_z r_z, \quad (2)$$

$$\partial^2 = f_{xx} r_x r_x + f_{yy} r_y r_y + f_{zz} r_z r_z + f_{xy} r_x r_y + f_{xz} r_x r_z + f_{yz} r_y r_z, \quad (3)$$

where ∂ and ∂^2 are the first and second radial derivatives; f_x , f_y , and f_z are the first derivatives in the x , y and z directions, respectively;

f_{ij} is the second derivatives value along ij direction.

The vector $r = (r_x, r_y, r_z)$ originates from the center toward the radial line of the sphere. We employed the normalized

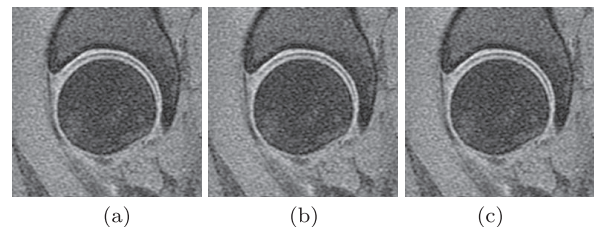


Fig. 2 Typical hip cartilage data sets acquired under continuous leg traction. Figures (a) to (c) are associated with three different datasets where traction was performed well, moderate, and poor, respectively. These datasets were regarded as GOOD, MODERATE, and POOR datasets in the experiments.

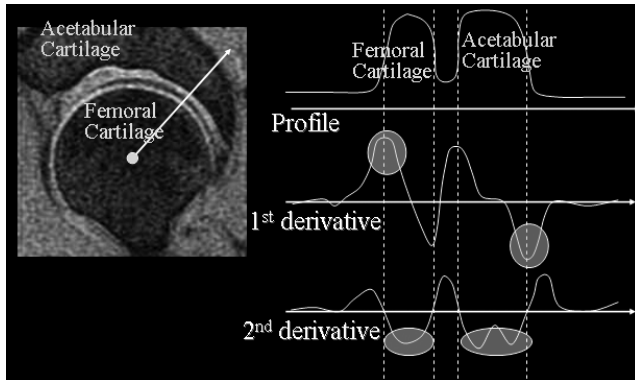


Fig. 3 Profile of femoral and acetabular cartilages and corresponding first and second derivatives along a radial line with respect to femur center are shown. As seen, the bony tissues appear dark and the soft tissues such as cartilages and muscles, appear bright.

in the operations. In this case, the magnitude of the gradient vector in the boundary of the femoral head and cartilage is large in the radial direction originating from the femoral head center. Figure 3 illustrates the profile of femoral and acetabular cartilages and corresponding first and second derivatives along a radial line with respect to femur center. The center is estimated using the orientation of the gradient vector at each voxel and the possible range of the femoral head radius by a Hough transform [18].

A typical example of the femoral head center estimation is shown in Fig. 4. Based on our previous work [20], we employ the estimated center as the center of a cube for selecting the region of interest. The size of the cube sides is determined as follows. As explained earlier, the femoral head typically is of a spherical shape with a radius of less than 25 mm. This is equivalent to a size of 80 ($25/0.03125$) slices in the re-sampled data sets. The cartilage thickness in typical cases is less than 5 mm, that is equivalent to a size of 16 ($5/0.03125$) slices in the resampled data sets [12]. Therefore, a cube with the estimated center location and dimensions of $((80 + 16) \times 2)^3$, i.e., $192 \times 192 \times 192$ voxels is regarded as the volume of interest for further operations.

2.2 Segmentation of Femoral Head and Acetabulum

In the previous works, 3D-filtering techniques and second directional derivative images were used to segment the acetabular and femoral head cartilages. However, the performance, computational cost and feasibility of the techniques were not adequately demonstrated [18], [20]. The proposed approach is a multi step algorithm based on the anatomical knowledge about the hip joint cartilages and bones. The hip cartilages are surrounded by the acetabulum and the femoral head. In many joint diseases, the cartilage damage is very common [30]–[36]. We have assumed that the edges of bones in the hip are more consistent than those of hip cartilages. For this reason, we first segment the bony tissues in the hip, i.e., the acetabulum and the femoral head. The

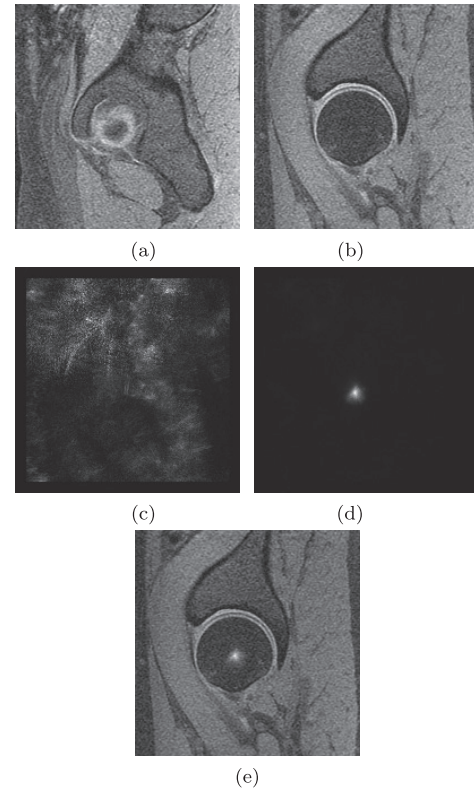


Fig. 4 Automatic estimation of femoral head center using the Hough transform and anatomical constraint of hip joint bones and cartilages [18]. (a) and (b) are associated with two typical MR slices of a hip joint in the early and middle locations of a sagittal direction. (c) and (d) are the hough spaces corresponding to (a) and (b), respectively. (e) The Hough transform in (d) and overlaid center with (b). This result demonstrates the effectiveness of the customized Hough transform of Sect. 2.1 in femoral head center estimation.

results are then employed for acetabular and femoral cartilage segmentation in later stages. Different segmentations techniques are reported in the literature [37]–[40]. In this research, we employ a singular value decomposition (SVD) technique [21]–[27][†] to segment the femoral head and the acetabulum in the hip. The steps of the proposed algorithm are explained in the following. Flowchart of the SVD technique is shown in Fig. 5.

2.2.1 Feature Analysis of Image Data

An MR data set is often affected by a partial volume effect. In this regard, we choose a local volume for each voxel [21]. We consider the gray values of each voxel and its surrounding neighbors to create a vector of 23 members. Such a vector is shown in Fig. 6. We aim to classify the hip bony tissues based on the corresponding feature vectors. To reduce the computational cost, a feature analysis of the local vectors is necessary [23]. We apply the principal component analysis (PCA) [24] to determine the effective dimension of

[†]This technique is a vector quantization clustering technique and is established based on the principle component analysis (PCA).

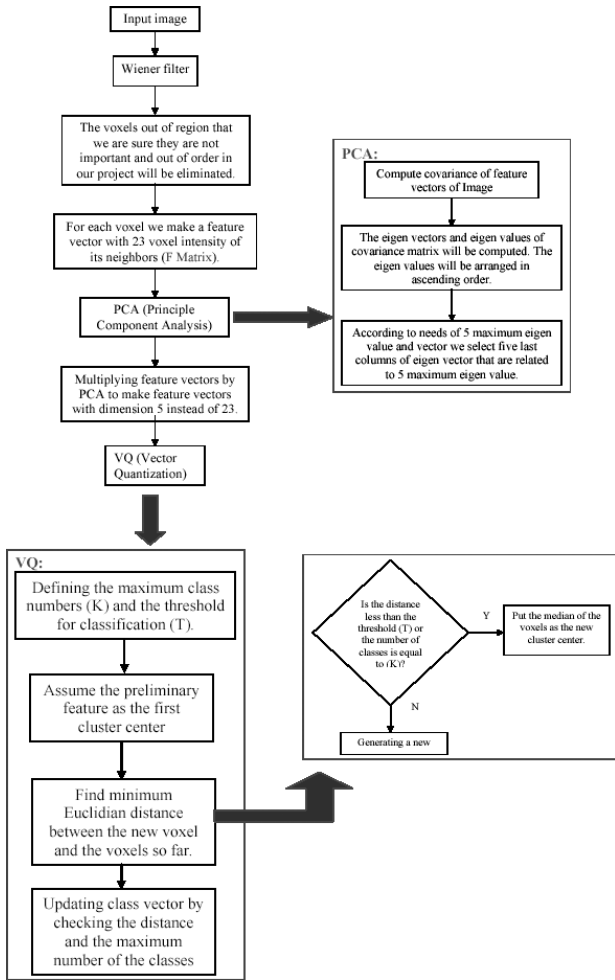


Fig. 5 Flowchart of the SVD algorithm discussed in Sect. 2.2.

the feature vectors by the associated orthogonal transformation matrix [i.e., the Karhunen-Loeve (K-L) transformation matrix]. In the available datasets, we have found that the total variance associated with the first five eigenvectors were equivalent to 92% of all Eigen vectors. Hence, a vector dimension of 5 is selected in the rest of operations. In a data set, calculating the K-L matrix for all voxels is very time consuming. We hence determine a general K-L matrix by employing several training samples. We then apply the result to segment all datasets acquired from the same source.

2.2.2 Vector Quantization Algorithm

As we discussed in Sect. 2.2.1, we apply the K-L transformation to the local vector series. In the K-L domain, the feature vectors are formed by the first five principal components from the transformed vector series. There are several approaches to classify the vectors [25]. We employ an unsupervised self-adaptive vector quantization (VQ) algorithm for handling the classification task. In the hip MR data sets, four classes including cartilage, muscle, bone and articular space are available. The partial volume effect (PVE) between nearby tissues should be considered as additional

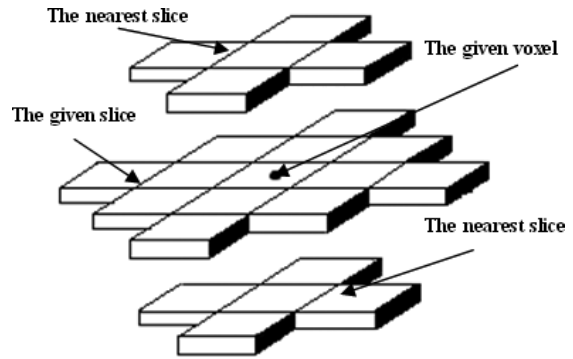


Fig. 6 The feature vector selected for bone segmentation. We selected 22 neighbors for each voxel in the datasets. Hence, a vector of 23 dimensions was employed for vector quantization algorithm. Details are discussed in Sect. 2.2.1.

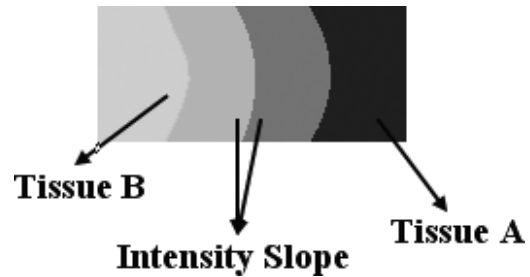


Fig. 7 Gradual variation of the intensity in nearby tissues denoted as A and B, respectively. The overlapped area associated with the partial volume effect. See Sect. 2.2.2 for details.

classes. Figure 7 illustrates an example of the (PVE). In the available MR data sets, muscle, bones, cartilages, and articular space are adjacent to each other. In this case, we have considered four additional classes in the operations. Therefore, a value of eight was assigned to the maximum class numbers and denoted as K. A threshold value of T, i.e., the vector similarity criteria, is another factor for discriminating the classes from each other. In the datasets, we have experimentally found that the square root of the component with the maximum variance in the feature vector is a good estimate for T. This allows the VQ algorithm to achieve the minimum class number with the maximum variance. Since T is estimated from the data, the employed VQ algorithm can be regarded as a self-adaptive algorithm. The VQ algorithm is similar to an unsupervised clustering algorithm. The number of classes and the representative vectors are updated continuously when more vectors are included in the calculation.

2.2.3 Bone Segmentation

In the employed data sets, the partial volume effect is found negligible. Therefore, after classification, the hip dataset is labeled into four classes including bone, PVE between bone and muscle, cartilage, and PVE between cartilage and bone. These four classes are enumerated as 1 to 4, respectively. Classes #1 and #3 are associated with the lowest

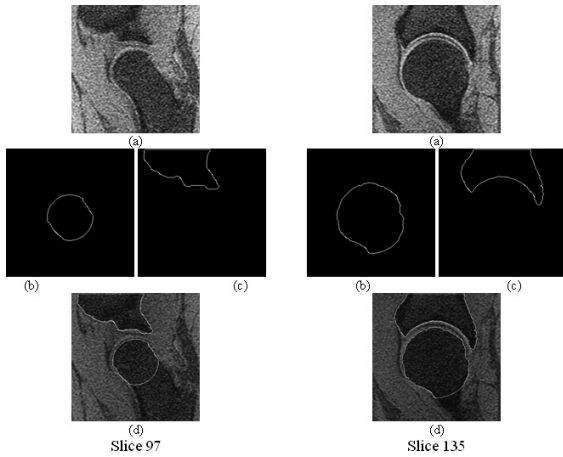


Fig. 8 Bone segmentation using the SVD technique. (a) Typical MR slices in two different locations of a hip joint are shown. (b) and (c) are associated with segmented acetabulum and femoral head, respectively. (d) The result is overlaid with original image.

and the highest intensities, respectively. These classes are hence easily segmented. Class #1 contains the acetabulum and femoral head. The next step is to segment these bones from each other. We follow the approach of our previous work [20] to address this problem. We fit a circle with the same center obtained in Sect. 2.1 to each slice of the data set. The extent of a femoral head is known in typical clinical cases [1]. The largest 3D component that is connected to the estimated center and is inside the estimated circle is automatically regarded as the femoral head. For segmenting the acetabulum, after excluding the femoral head from the whole binary data set, the largest and closest connected component corresponding to the femoral head upper boundary is segmented as acetabulum. Figure 8 shows typical examples applying the proposed SVD algorithm.

2.3 Localization of the Articular Space

The Canny operator was used to be an optimal edge detector to tracked intensity discontinuities [41]. The tracking process of canny exhibits hysteresis controlled by two thresholds: T_1 and T_2 with $T_1 > T_2$. This hysteresis helps to ensure that noisy edges are not broken up into multiple edge fragments. We apply a Canny operator to the results obtained from the first radial derivative in Sect. 2.1. We have experimentally found that the Canny operator is also effective to track the intensity discontinuities in the articular space [41], [42]. In the available datasets, the normalized thresholds of $T_1=0.4$ and $T_2=0.2$ are utilized to enhance the edges. The mentioned filter is applied to the original data, first and second directional derivative images which results in binary images containing bony and soft tissue’s edges. Then, a multi-step technique including the simple logical operations and morphological operations with the concern of the anatomical constraints (the femoral head center position and the extent of the hip joint space in the datasets) is employed to localize the articular space central line. The

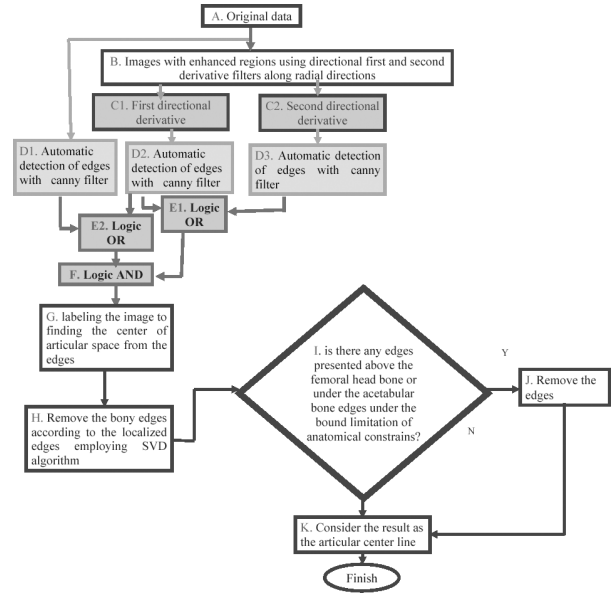


Fig. 9 Articular central line localization using the Canny edge detector and logical operation.

detailed algorithm is shown in Fig. 9 and a typical result is shown in Fig. 10.

2.4 Segmentation of Acetabular and Femoral Head Cartilages

In this step, to segment the cartilages the top-hat transform combined with first derivative of the images. Wiener filtering is a nonlinear operation often used for reducing the noise and preserve edge simultaneously [28], [29]. The image is viewed as a surface, with mountain (high intensity) and valleys (low intensity). It is desirable to maximize the contrast of objects of interest for minimizing the number of valleys. The contrast enhancement technique is the combined use of the top-hat transforms. The opening operation is anti-extensive, i.e. grey scale of every pixel in the opening processed image is not greater than that in the original image, and lighter objects smaller than structuring element will be erased by opening operation. So the residual between original image and opening image can be defined as top-hat transform. The structure element in this approach defined as a flat, disk-shaped; with radius 3 that is shown in Fig. 11. The disk-shaped structuring element is approximated by a sequence of N periodic-line structuring elements. When N equals 0, no approximation is used, and the structuring element members consist of all pixels whose centers are no greater than R away from the origin. In this approach N was specified 4. The top-hat image contains the “peaks” of objects that fit the structuring element. To maximize the contrast between the objects and the gaps that separate them from each other, the “top-hat” image is subtracted from the “original” image. Applying the top-hat filter to the original images lead to the rough segmentation of the regions with high contrast included the femoral head and acetabu-

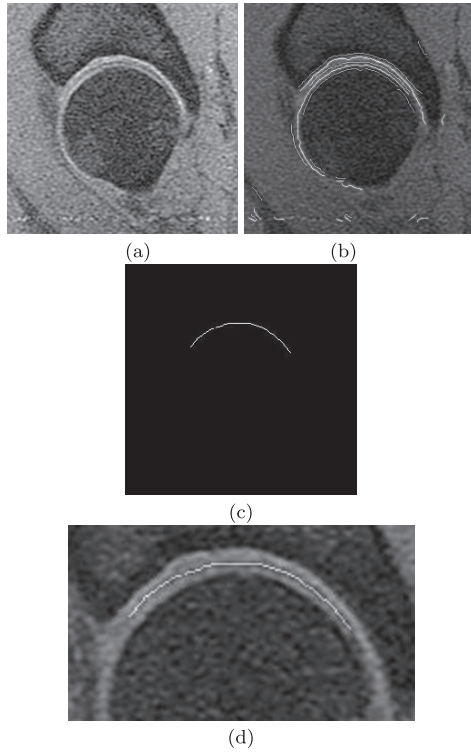


Fig. 10 Articular space central line localization. (a) Typical MR slice of a hip joint. (b) A Canny edge detector was applied to the filtered image obtained by calculating the first directional derivative introduced in Sect. 2.1. (c) Localized central line of the articular space by utilizing the anatomical constraint. (d) The localized articular space central line is overlaid with original image. See Sect. 2.3 for details.

lar cartilages and scattered pixels which are corresponded to the mussels. The scattered points can easily be removed from the images considering the restriction of the anatomical position of the hip joint cartilages. After that, the result is the segmented acetabular and femoral head cartilages which are connected to each other. Consequently, employing the articular space central line which is in the middle of the cartilages and applying two simple if conditions on the radius and angle of the segmented pixels originating from the femoral head center, lead to separation of the cartilages. The results of this step are shown in Fig. 12.

2.5 Thickness Map Generation of the Cartilages

Having the edges of acetabular and femoral head cartilages, the inner and outer boundaries of them are provided. Concerning the spherical shape of femoral head and this fact that the cartilages are bonded in the united center spheres, estimation of the thickness along the radial direction is more accurate than measuring it along normal directions of each pixel [43]. Thus, the thickness of each cartilage is estimated applying the Euclidian distance transform along the femoral head radial direction. To visualize the thickness map of the cartilages, the lightening and color were assigned to each voxel of the cartilages according to their thickness. The

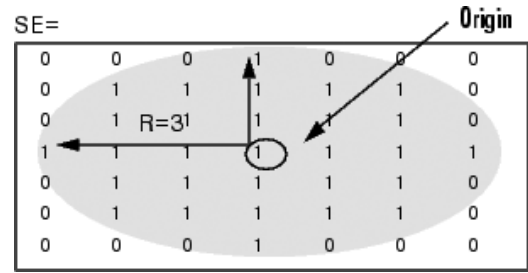


Fig. 11 The structure element defined as a flat, disk-shaped and a radius of 3 pixels in Sect. 2.4.

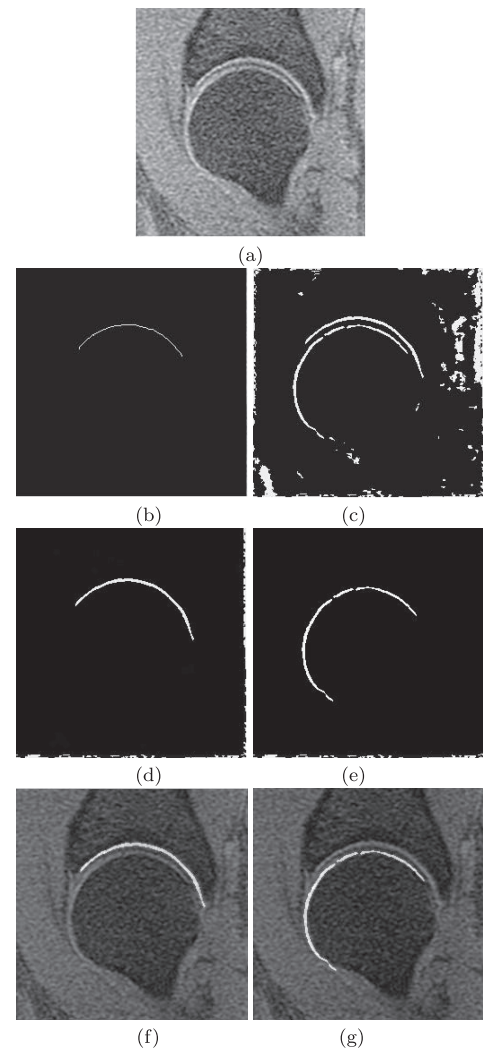


Fig. 12 Segmentation of the hip cartilages. (a) A hip joint slice. (b) The localized central line of articular space. (c) Rough segmentation of the hip joint cartilages. (d) and (e) show segmented acetabular and femoral cartilages, respectively. In (f) and (g) the original image is overlaid with the cartilages.

range of the color changes is from blue to red to show low and high thicknesses.

3. Results

3.1 Data Set

MR imaging was performed with fat-suppressed 3D fast spoiled gradient echo (SPGR) sequence using a unilateral surface coil (TORSO, General Electric, Milwaukee, WI) on a 1.5-T MR system (Horizon, General Electric). Imaging parameters were as follows: TR/TE , 24.4/5.7 ms; flip angle, 20 degrees, section thickness, 1.5 mm; in-plane resolution, 0.625 mm; imaging matrix, 256×256 ; signal acquisition, 2; imaging direction, sagittal. Imaging time was 10 min and 17 seconds. The proposed method applied to 40 sets (2400 images) of in-vivo MR data of normal and diseased hip joints. We classified the datasets into three categories of GOOD, MODERATE and POOR datasets based on considering several factors such as the quality of traction during data acquisition, anatomical constraint such as vicinity of the pelvis and the femur, shape and level of femoral head malformation, non-uniformity of bone intensity, level of discrimination between the femoral and acetabular cartilages and the contrast between the different tissues. In this study, we developed the techniques described in Sect. 2.1 in C++ language and the techniques of Sects. 2.2 to 2.5 in MATLAB. The experiments were performed on a Pentium IV (3 GHz, 512 Mbytes of RAM and 120 GB of memory) personal computer (PC). The time required for each step of the process is indicated in Table 1.

3.2 Assessment of the Method

We employed the proposed techniques to segment and visualize the hip cartilage. As mentioned in Section [2] the flowchart of the assessments is shown in Fig. 1. We evaluated the performance of the developed techniques on 40 hip joints of actual patients. Typical GOOD, MODERATE and POOR dataset are shown in Fig. 2. As seen, in a GOOD dataset traction was performed well and the hip articular space is well differentiated with respect to nearby cartilages. In a POOR dataset, the image has low contrast in the hip joint and traction failed to obtain successful results. In addition, in some POOR datasets the femoral head bone has unusual shape. In this case, femur center estimation based on assuming a spherical surface for femoral head is not appropriate. In practice, we employed 5 GOOD and 28 MODERATE datasets for the experiments and remaining POOR datasets were not participated in the evaluation procedures. The various steps of the algorithm are evaluated separately.

Table 1 Required time for the technique in the study.

Proposed techniques	Time (s)
Preprocessing	310
Bone segmentation	80
Articular central line localization	50
Cartilage segmentation	70
Cartilage thickness estimation and visualization	400

First to evaluate the applied algorithm for bone segmentation, we compared it with the previous method [20] based on Otsu’s adaptive thresholding [19] according to the manual segmentations, in ROC diagrams. Manual segmentation of 40 hip joints (20×2) was conducted by two experts. The success and failure of the algorithm is measured by finding the true positive rate (TPR) and false positive rate (FPR) in comparison with the previous method. In order to find the TPR we have to verdict the value of the true positive (TP) and the false negative (FN) and to define the FPR we have to decide the true negative (TN) and the false positive (FP). These values were corresponding to the four following types of tissues: (1) TP pixels (P_{TP}): correctly segmented bone tissues; (2) FP pixels (P_{FP}): non bone tissues recognized as bone tissues due to the failure of the technique; (3) FN pixels (P_{FN}) missed bone tissues; (4) TN pixels (P_{TN}): correctly did not segment as bone tissues. The examples of typical counting the FP, TP, FN and TN pixels are shown in Fig. 13.

A cube of dimensions $205 \times 20 \times 140$ assumed as a frame to count these parameters for each dataset. This region of interest is an area that has the most probability of consisting bony tissues. Thus in a typical dataset we have totally 5,883,500 pixels which are used for estimating the TP, FP, TN and FN. Tables 2, 3 and 4 show the defined parameters for optimal threshold in SVD algorithm in 5 GOOD, 8 MODERATE and ALL data sets respectively. To draw the ROC curve for the proposed algorithm, T is changed from 0.1 to its optimum value mentioned in Sect. 2.2 part B and for previous method [20] we draw it by increasing the window size of filters from 3 to 15 by double steps. The TPR and FPR are measured with the below formulas:

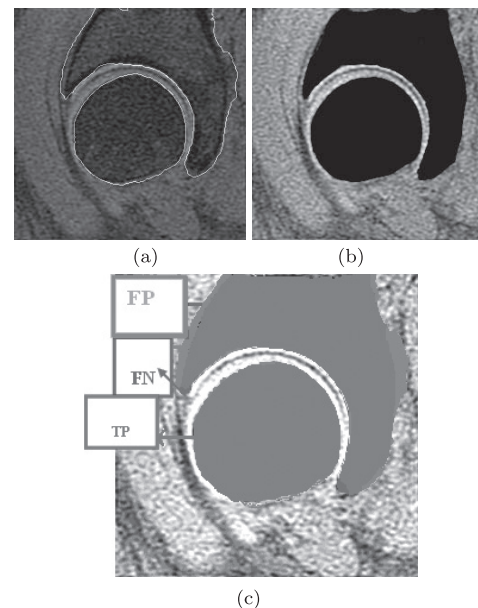


Fig. 13 Estimating the TP, FP, TN and FN parameters. (a) The result of the SVD algorithm, (b) The manual segmentation of the bony tissues and (c) The overlay of (a) and (b) that showed the TP in red, FP in blue and FN in green.

Table 2 Assessment of the bone segmentation with the proposed SVD algorithm is shown. Five GOOD datasets with optimal threshold T were selected in the experiments.

Good Dataset	TPR	FPR
1	0.91352	0.45955
2	0.91345	0.46042
3	0.91321	0.46111
4	0.91289	0.46197
5	0.91250	0.46287
Average	0.91312	0.46118

Table 3 Explanation is the same as Table 2. Eight MODERATE datasets with optimal threshold T were selected in the experiments.

Moderate Dataset	TPR	FPR
1	0.90470	0.56003
2	0.90438	0.56165
3	0.90405	0.56262
4	0.90386	0.56340
5	0.90360	0.56403
6	0.90334	0.56504
7	0.90302	0.56603
8	0.90256	0.56699
Average	0.90369	0.56373

Table 4 Explanation is the same as Table 2. ALL datasets with optimal threshold T are participated in the experiments.

ALL Datasets	TPR	FPR
Final Average	0.90731	0.52428

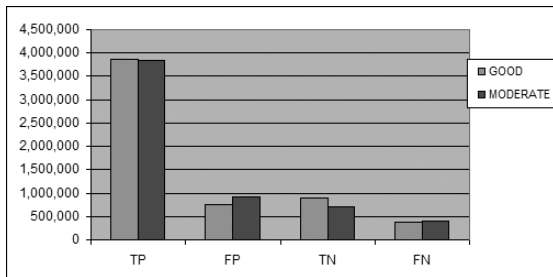


Fig. 14 The comparison between the SVD method and the Otsu's adaptive thresholding algorithm [20] applied to the 5 GOOD and 28 MODERATE data sets.

$TPR = \frac{TP}{(TP+FN)}$; $fPR = \frac{FP}{(FP+TN)}$. The diagram is shown in Fig. 14 compares the SVD method proposed for bone segmentation with our previous method [20].

The ROC diagrams are shown in Fig. 15 for GOOD, MODERATE and ALL data sets separately. As can be seen in the diagrams the results of the proposed algorithm are in general better than the previous one because the entire method is done in 3D manner on the voxels. Also, the results illustrate the supremacy of the vector quantization (SVD) technique in some slices which had inaccurate results in the previous method. In SVD technique, for segmenting the bone, we have defined two constraints: a threshold for classification (T) and the maximum number of the classes (K). With these two constraints we considered the distance restriction on the feature vectors and the image attribute. To assess the algorithm used for the articular central line localization and cartilage segmentation, we used the TP, FP,

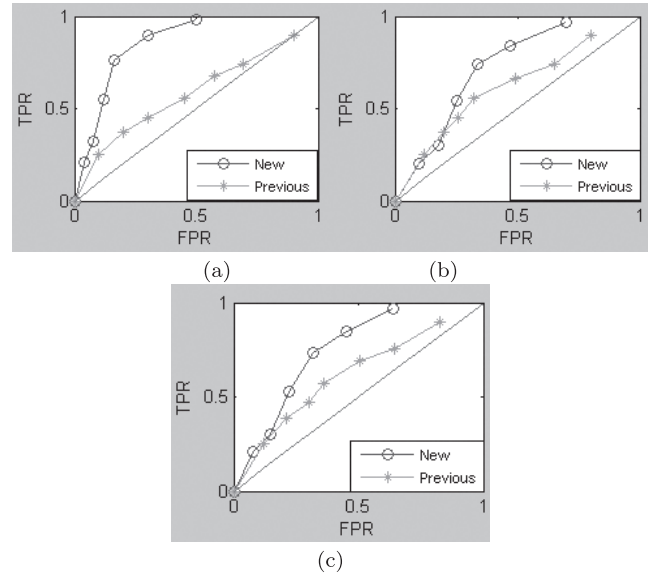


Fig. 15 The ROC curve to compare the SVD algorithm illustrated in Sect. 2.1 and previous method based on otsu's adaptive thresholding [20]. The blue curves correspond to the SVD method and green curves show the result of thresholding method in (a) GOOD, (b) MODERATE, and (c) ALL datasets. The red line is $x=y$.

TN and FN pixels to measure the SUCCESS and ERROR of the algorithm as follow: (1) Success rate of segmentation technique was computed by $SUCCESS = (\frac{TP}{P_{ref}}) \times 100$. (2) Error was determined by $ERROR = (\frac{FP+FN}{P_{ref}}) \times 100$.

Hence, for each slice of a data set, the localized central line/ cartilages pixels, that was selected by all two experts as the articular space central line/ cartilages, were used as the reference and denoted as P_{ref} . 3) Central line localization/ cartilages segmentation performance was classified into one of the three groups: good, moderate, and poor. If ($SUCCESS > 90\%$) and ($ERROR < 10\%$), localization performance was good. If ($SUCCESS > 70\%$) and ($ERROR < 20\%$), localization performance was moderate. Otherwise localization performance was poor. The capability of the technique for localizing the articular space central line and segmenting the cartilages are illustrated in Tables 5 and 6. The algorithm is not well done in some slices of the data sets. The reasons are as follows: 1. The bad traction that makes it difficult to separate the acetabular and femoral head cartilages very carefully.

2. The deformable femoral head and acetabulum in the joints; the fully automatic method discussed in this paper is based on the anatomical constraint like femoral head center, thus in the data sets that the femoral head is too deform this technique may failed. 3. The noise of imaging is the other problem: In segmentation approaches were illustrated we used smoothing filter to reduce the noise, but in some data sets the noise is too much that these filters can not solve our problem. 4. The ligament that reinforces the femoral head in its place, has the same intensity with cartilage and may cause reduction of accuracy in segmenting the cartilages [1]. Table 7 summarizes the performance of

Table 5 Assessment of the proposed method for articular space central line localization in the presence of 5 GOOD datasets and 28 MODERATE datasets. For each dataset, 140 slices was participated in the experiments.

	Good outcome %	Moderate outcome %	Poor outcome %
Good Data	97(1629/1680)	2(33/1680)	1(18/1680)
Moderate Data	91(2675/2940)	8(235/2940)	1(29/2940)
All Data	93(4304/4620)	6(268/4620)	1(47/4620)

Table 6 Assessment of the proposed cartilage segmentation technique in the presence of 5 GOOD datasets and 28 MODERATE datasets. For each dataset, 140 slices was participated in the experiments.

	Good outcome %	Moderate outcome %	Poor outcome %
Good Data	88(1474/1680)	10(168/1680)	2(33/1680)
Moderate Data	79(2322/2940)	12(352/2940)	9(264/2940)
All Data	82(3796/4620)	12(520/4620)	6(297/4620)

Table 7 Assessment of the entire steps of proposed technique in the presence of 5 GOOD and 28 MODERATE datasets. For each dataset, 140 slices was participated in the experiments.

	Good outcome %	Moderate outcome %	Poor outcome %
Bone Segmentation	96(32/33 Datasets)	3(1/33 Dataset)	1(46/4620 Slices)
Articular space central line localization	93(31/33 Datasets)	6(2/33 Datasets)	1(46/4620 Slices)
Cartilage Segmentation	82(27/33 Datasets)	12(4/33 Datasets)	6(2/33 Datasets)

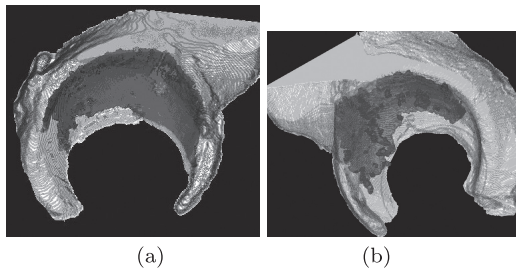


Fig. 16 Thickness maps of the segmented acetabular cartilages. (a) A GOOD data set. (b) A MODERATE dataset. Green (light grey), red (moderate grey) and blue (dark grey) are associated with high (larger than 4 mm), medium (between 2 to 4 mm) and low thicknesses (lower than 2 mm) of the cartilage, respectively.

varied steps of the algorithm for all 33 datasets. For each dataset 140 slices which may consist of cartilages that is known in typical cases, are selected and the percentages are shown with division of number of correct slices to all the dataset’s slices. The 3D visualization of two cartilage thickness maps picked from GOOD, MODERATE data sets are shown in Fig. 16.

4. Conclusions

We developed an automatic method for segmentation and surface rendering of hip joint cartilages from MR images. In the proposed approach, we employed continuous leg traction technique to allow clear separation of the acetabular and femoral head cartilages. Moreover, we combined the vector quantization and PCA algorithms for bone segmentation. We also customized the double thresholding canny edge detector filter and anatomical constraint of the hip joint to localize the articular space central line. We tailored an accurate localized articular space central line with top-hat filters to segment the hip joint cartilages. The thickness map of

segmented cartilages was rendered employing the marching cube algorithm that produces a triangle mesh by computing iso-surfaces from discrete data. The surface represents by connecting the patches from all cubes on the iso-surface boundary. In the presence of available data sets, the results were promising. We quantify the new method for bone segmentation in ROC diagrams in comparison with the previous segmentation technique based on Otsu’s thresholding [20]. We experimentally showed that the proposed method in the presence of the available data sets showed effective in 90.5% of the slices for cartilage segmentation, applying the SUCCESS and ERROR formulas. Accurate localization of the articular space central line is strong point that leads to better and more precision cartilage segmentation results. The evaluation was subjectively made by two experts. The failure of the algorithm in the remaining slices was mainly due to poor imaging condition, incomplete traction, and irregularity in the spherical shape of bony and cartilage tissues. In such cases, even the judgment of an expert in determining the exact location of the articular space was uncertain. The consideration of improving methods of the MR imaging conditions in the case of low contrast could make a POOR data set to MODERATE dataset. One major concern of the developed algorithm is speed. The time required for performing full automatic localization, classification, and visualization of a data set including 192 slices [size: 256×256 pixels] was around 15 minutes. By employing a multi-CPU machine, and developing a multi-thread programming, this concern must be addressed in our future work. We as well need to evaluate the algorithms with more data sets, integrate the proposed technique in a software package for cartilage segmentation, cartilage thickness map estimation and corresponding 3D visualizations that handles clinical tasks for quantification of hip joint cartilages.

References

- [1] F. Cicutinni, A. Forbes, K. Morris, N. Woodford, and S. Stuckey, "Determining the volume of hip cartilage by magnetic resonance imaging," *Radiography*, no.6, pp.79–82, 2000.
- [2] L. Yahia-Cherif, B. Gilles, T. Molet, and N. Magnenat-Thalmann, "Motion capture and visualization of the hip joint with dynamic MRI and optical systems," *J. Visualization and Computer Animation*, vol.15, no.3–4, pp.377–385, 2004.
- [3] M. Mlejnek, A. Vilanova, and M.E. Groller, "Interactive thickness visualization of articular cartilage," *IEEE Trans. Visualization*, pp.521–528, 2004.
- [4] A. Lch, E. Eckstein, M. Haubner, and K.-H. Englmeier, "A non-invasive technique for 3-dimensional assessment of articular cartilage thickness based on MRI part 1: Development of a computational method," *Magnetic Resonance Imaging*, vol.15, no.7, pp.795–804, 1997.
- [5] C. Kauffmann, P. Gravel, B. Godbout, A. Gravel, G. Beaudoin, J.P. Raynauld, J. Martel-Pelletier, J.P. Pelletier, and J.A. de Guise, "Computer-aided method for quantification of cartilage thickness and volume changes using MRI: Validation study using a synthetic model," *IEEE Trans. Biomed. Eng.*, vol.50, no.8, pp.978–988, 2003.
- [6] A. Accardo, G. Candido, V. Jellus, R. Toffanin, and F. Vittur, "Ex vivo assessment of trabecular bone structure from three-dimensional projection reconstruction MR micro-images," *IEEE Trans. Biomed. Eng.*, vol.50, pp.967–977, 2003.
- [7] E.J. McWalter, W. Wirth, M. Siebert, R.V.M. Hudelmaier, D.R. Wilson, and F. Eckstein, "Use of novel interactive input devices for segmentation of articular cartilage from magnetic resonance images," *Osteoarthritis and Cartilage*, vol.13, pp.48–53, 2005.
- [8] P. Kornaat, S. Reeder, S. Koo, J. Brittain, H. Yu, T. Andriacchi, and G. Gold, "MR imaging of articular cartilage at 1.5 T and 3.0 T: Comparison of SPGR and SSFP sequences," *Osteoarthritis and Cartilage*, vol.13, pp.338–344, 2005.
- [9] T. Nishii, K. Nakanishi, N. Sugano, H. Naito, S. Tamura, and T. Ochi, "Acetabular labral tears: Contrast-enhanced MR imaging under continuous leg traction," *Skeletal Radiology*, vol.25, pp.349–356, 1996.
- [10] Y. Sato, K. Nakanishi, and H. Tanaka, "A fully automated method for segmentation and thickness determination of hip joint cartilage from 3D MR data," *Proc. CARS International Congress Series*, vol.1230, pp.352–358, 2001.
- [11] R.A. Zoroofi, Y. Sato, T. Sasama, T. Nishii, N. Sugano, K. Yonenobu, H. Yoshikawa, and S. Tamura, "Automated segmentation of acetabulum and femoral head from 3-D CT images," *IEEE Trans. Inf. Technol. Biomed.*, vol.7, no.4, pp.329–343, 2003.
- [12] T. Nishii, N. Sugano, and Y. Sato, "Three-dimensional distribution of acetabular cartilage thickness in patients with hip dysplasia: A fully automated computational analysis of MR imaging," *Osteoarthritis and Cartilage*, vol.12, pp.650–657, 2004.
- [13] T. Nishii, K. Nakanishi, N. Sugano, K. Masuhara, K. Ohzono, and T. Ochi, "Articular cartilage evaluation in osteoarthritis of the hip with MR imaging under continuous leg traction," *Magnetic Resonance Imaging*, vol.16, no.8, pp.871–875, 1998.
- [14] T. Stammberger, F. Eckstein, M. Michaelis, K.-H. Englmeier, and M. Resier, "Interobserver reproducibility of quantitative cartilage measurements: Comparison of B-spline snakes and manual segmentation," *Magnetic Resonance Imaging*, vol.17, no.7, pp.1033–1042, 1999.
- [15] L. Antoniadis, T.D. Spector, and A.J. MacGregor, "The genetic contribution to hip joint morphometry and relationship to hip cartilage thickness," *Osteoarthritis and Cartilage*, vol.9, no.6, pp.593–595, 2001.
- [16] J. Hohe, S. Faber, R. Muehlbauer, M. Reiser, K.-H. Englmeier, and F. Eckstein, "Three-dimensional analysis and visualization of regional MR signal intensity distribution of articular cartilage," *Medical Engineering & Physics*, no.24, pp.219–227, 2002.
- [17] J. Cheong, D. Suter, and F. Cicutinni, "Development of semi-automatic segmentation methods for measuring tibial cartilage volume," *IEE Proc., Digital Imaging Computing*, pp.307–314, 2005.
- [18] Y. Sato, T. Kubota, K. Nakanishi, H. Tanaka, N. Sugano, T. Nishii, K. Ohzono, H. Nakamura, T. Ochi, and S. Tamura, "Three-dimensional reconstruction and quantification of hip joint cartilages from magnetic resonance images," *Lecture Notes in Computer Science*, vol.1679, pp.338–347, 1999.
- [19] N. Otsu, "A threshold selection method from gray level histograms," *IEEE Trans. Syst. Man Cybern.*, vol.9, no.1, pp.62–66, 1979.
- [20] R.A. Zoroofi, Y. Sato, T. Nishii, K. Nakanishi, H. Tanaka, N. Sugano, H. Yoshikawa, H. Nakamura, and S. Tamura, "Automated segmentation of acetabular cartilage in MR images of the hip," *IEICE Technical Report*, MI2005-42(2005-9), 2005.
- [21] T.N. Papps, "An adaptive clustering algorithm for image segmentation," *IEEE Trans. Signal Process.*, vol.40, no.4, pp.901–914, 1992.
- [22] J. Zhang, J.W. Modestino, and D.A. Langan, "Maximum-likelihood parameter estimation for unsupervised stochastic model-based image segmentation," *IEEE Trans. Image Process.*, vol.3, no.4, pp.404–420, 1994.
- [23] K. Fukunaga, *Introduction to Statistical Pattern Recognition*, 2nd ed., Academic, New York, 1990.
- [24] C. Chatfield and A.J. Collins, *Introduction to Multivariate Analysis*, Chapman & Hall, London, U.K., 1980.
- [25] A. Gersho and R.M. Gray, *Vector Quantization and Signal Compression*, Kluwer, Boston, MA, 1992.
- [26] Y. Linde, A. Buzo, and R.M. Gray, "An algorithm for vector quantizer designed," *IEEE Trans. Commun.*, vol.28, no.1, pp.84–95, 1980.
- [27] W. Feller, *An Introduction to Probability Theory and its Applications*, 3rd ed., Wiley, New York, 1968.
- [28] W. Li-qiang, N. Xu-xiang, L. Zu-kang, Z.H. Xu-feng, et al., "Enhancing the quality metric of protein microarray image," *Journal of Zhejiang University SCIENCE*, vol.5, no.12, pp.1621–1628, 2004.
- [29] A. Movafeghi, M. Taheri, M.H. Kargarnovin, et al., "Quality improvement of digitized radiographs by filtering technique development based on morphological transformations," *IEEE Nuclear Science Symposium Conference*, vol.3, pp.1846–1849, 2004.
- [30] H. Ito, T. Matsuno, and K. Kaneda, "Prognosis of early stage avascular necrosis of the femoral head," *Clinical Orthopedics*, vol.358, pp.149–157, 1999.
- [31] K. Takaoka, K. Ohzono, M. Matsui, K. Masuhara, and K. Ono, "Prognostication of non-traumatic avascular necrosis of the femoral head," *Clinical Orthopedics*, vol.303, pp.155–164, 1994.
- [32] A.J. Holman, G.C. Gardner, M.L. Richardson, and P.A. Simkin, "Quantitative magnetic resonance imaging predicts clinical outcome of core decompression for osteonecrosis of the femoral head," *J Rheumatology*, vol.22, no.10, pp.1929–1933, 1995.
- [33] K.H. Koo and R. Kim, "Quantifying the extent of osteonecrosis of the femoral head," *J Bone Joint Surgery*, vol.77, no.6, pp.875–880, 1995.
- [34] J. Gougoutas, J. Wheaton, A. Borthakur, M. Shapiro, B. Kneeland, K. Udupa, and R. Reddy, "Cartilage volume quantification via live wire segmentation," *Academic Radiology*, vol.11, no.12, pp.1389–1395, 2004.
- [35] H.J. Mankin, "Non-traumatic necrosis of bone (osteonecrosis)," *N Eng J Med*, vol.326, p.1473, 1992.
- [36] Y.M. Kim, J.H. Ahn, H.S. Kang, and H.J. Kim, "Estimation of the extent of osteonecrosis of the femoral head using MRI," *J Bone Joint Surgery*, vol.80, pp.954–958, 1998.
- [37] M.E. Steinberg, "Avascular necrosis: Diagnosis, staging, and management," *J Musculoskeletal Med*, vol.14, no.11, pp.13–25, 1997.
- [38] J.G. Snel, H.W. Venema, and C.A. Grimbergen, "Detection of the carpal bone contours from 3-D MR images of the wrist using a planar radial scale-space snake," *IEEE Trans. Med. Imaging*, vol.17, no.6, pp.1063–1072, 1998.

- [39] Y. Kang, K. Engelke, and W.A. Kalender, "A new accurate and precise 3-D segmentation method for skeletal structures in volumetric CT data," *IEEE Trans. Med. Imaging*, vol.22, no.5, pp.586–598, 2003.
- [40] H. Lu, Z. Liang, B. Li, X. Li, J. Meng, and X. Liu, "Mixture-based bone segmentation and its application in computer aided diagnosis and treatment planning," *IEEE Proc. Third Int. Conf. on Image and Graphics*, 2004.
- [41] N.R. Pal and S.K. Pal, "A review of image segmentation techniques," *Pattern Recognit.*, vol.26, pp.1277–1294, 1993.
- [42] M. Khanmohammadi, R.A. Zoroofi, Y. Sato, T. Nishii, K. Nakanishi, H. Tanaka, N. Sugano, H. Yoshikawa, H. Nakamura, and S. Tamura, "Automated segmentation of the articular space in MR images of the hip joint," *IET International Conference on Visual Information Engineering*, pp.500–505, 2006.
- [43] Y. Sato, H. Tanaka, T. Nishii, K. Nakanishi, N. Sugano, T. Kubota, H. Nakamura, H. Yoshikawa, T. Ochi, and S. Tamura, "Limits on the accuracy of 3D thickness measurement in magnetic resonance images—Effects of voxel anisotropy," *IEEE Trans. Med. Imaging*, vol.22, no.9, pp.1076–1088, 2003.



Mahdiah Khanmohammadi was born in Arak, Iran, in 1982. She graduated from Farzanegan High School, Affiliated to National Organization for Development of Exceptional Talents (NODET) (major: Mathematics-Physics) in 1999. She passed the entrance examination of engineering universities of Iran with a rank of 61 (out of 750,000 participants) in 1999, and joined Amirkabir University of Technology, Tehran, IRAN. She received the B.Sc. degree in Biomedical Engineering (major: Bio-

electric) from Amirkabir University of Technology, in 2004. In 2005, she joined University of Tehran, Tehran, Iran and received the M.Sc. degree in Biomedical Engineering (major: Bioelectric) in 2007. From 2006 till now, she also collaborated at Biomedical Engineering Division of Arak Medical University, Iran, as a Senior Medical instrument investigator.



Reza Aghaiezhadeh Zoroofi received the B.S. degree in Electronic Engineering from Amir-Kabir University, Tehran, Iran, the M.S. degree in Telecommunication Engineering from Khajeh Nassir University, Tehran, Iran, and the Ph.D. degree in Medical Science from Osaka University, Osaka, Japan, in 1989, 1991, and 1998, respectively. From January to March 1997, he was a NEDO Researcher at Mechanical Engineering Laboratory, Ministry of International Trade and Industry, Tsukuba, Japan.

From April 1997 to March 1998, he was a Research Fellow at the National Cardio-vascular Center Research Institute, Osaka. From April 1998 to March 2000, he was a JSPS Postdoctoral Fellow in the Division of Functional Diagnostic Imaging, Osaka University Medical School. In April 2000, Dr. Zoroofi joined the School of Electrical and Computer Engineering, Faculty of Engineering, University of Tehran, Iran where he is currently working as an Associate Professor. In summers 2000 to 2007, Dr. Zoroofi collaborated at Osaka University Medical School as Invited Research Scholar and Invited Associate Professor. His research activities include works in the fields of medical image analysis and medical software development.



Takashi Nishii received his M.D. and Ph.D. degrees from Osaka University, Japan in 1989 and 1997 respectively. From 1989 to 1993, he received training for a medical doctor in Osaka University Hospital and other city hospital. From 1993 to 1997, he was a graduate student of Osaka University Graduate School of Medicine. From 1998 to 2008, he was an assistant professor of Department of Orthopaedic Surgery, Osaka University Graduate School of Medicine. He is currently an associate profes-

sor of Department of Orthopaedic Medical Engineering, Osaka University Graduate School of Medicine. His research interests include joint arthroplasty, image analysis, computer analysis, and biomechanical analysis in the field of orthopaedic surgery. He is a member of Japanese Orthopaedic Association, Orthopaedic Research Society, and International Society for Magnetic Resonance in Medicine.



Hisashi Tanaka received his B.E. and M.E. degrees in Nuclear Engineering from Tokyo University, Japan in 1983 and 1985 respectively. He also received his M.D. and PhD degrees in Medicine from Osaka University, Japan in 1991 and 2006 respectively. From 1991 to 1995, he was a resident in Radiology at Osaka Rosai Hospital and Osaka University Hospital. From 1995 to 1996, he worked as a visiting scientist and visiting assistant professor at University of Rochester Medical Center in Rochester

NY. After completing fellowship in radiology during 1996 and 1997 at Osaka University Hospital, he joined the Department of Radiology of Osaka University Graduate School of Medicine as a faculty member. He is currently an Associate Professor at the department. His research interests include imaging in joint structures and the central nervous system. Dr Tanaka is a member of the Radiological Society of North America.



Yoshinobu Sato received his B.S., M.S. and Ph.D. degrees in Information and Computer Sciences from Osaka University, Japan in 1982, 1984, 1988 respectively. From 1988 to 1992, he was a Research Engineer at the NTT Human Interface Laboratories. In 1992, he joined the Division of Functional Diagnostic Imaging of Osaka University Medical School as a faculty member. From 1996 to 1997, he was a Research Fellow in the Surgical Planning Laboratory, Harvard Medical School and Brigham and

Women's Hospital. He is currently an Associate Professor at Osaka University Graduate School of Medicine and an Adjunct Associate Professor at Graduate School of Information Science and Technology, Osaka University. His research interests include medical image analysis, computer assisted surgery, and computational anatomy. Dr. Sato is a member of IEEE, MICCAI, and CAOS-International, and an editorial board member of *Medical Image Analysis* and the *International Journal of Computer Assisted Radiology and Surgery*.